Article

Bioinspired Sarcomeric Double-Network Hydrogels for Programmable Mechanics with Ultralow Hysteresis

Yang Luo *

Posted Date: 12 May 2026

doi: 10.20944/preprints202605.0810.v1

Keywords: double-network hydrogel; ultra-low hysteresis; electrical signal; freeze-resistance; smart materials

 doi:10.20944/preprints202605.0810.v1

Article

Bioinspired Sarcomeric Double-Network Hydrogels for Programmable Mechanics with Ultralow Hysteresis

Yang Luo [1,2]

[1] Department of Mathematics and Physics, North China Electric Power University, Hebei, 071003, China; luoyang@pku.org.cn

[2] Hebei Key Laboratory of Physics and Energy Technology, Hebei, 071003, China

Abstract

Hysteresis is normally unavoidable in hydrogels under complex external loading conditions due to the intermolecular friction, which usually leads to fatigue. Here, we develop a sarcomere-inspired double-network hydrogel made from polyacrylamide, alginate and phytic acid, whose hysteresis can be precisely modulated by preloading. Particularly, due to the synergy of micellization, fibrillation and micro-lubrication, the as-prepared hydrogel displays an ultra-low hysteresis (≤ 0.02 %) after it experiences a pre-tensile process at a specific amplitude and strain rate, or even possesses negative hysteresis in the case of low tensile amplitudes or high strain rates. Interestingly, smart responses of the developed hydrogel to cyclic tensile loadingare similar to the mechanical behaviors of sarcomeres in vivo. Likewise, the derived hydrogel with ultra-low hysteresis performs reliably even at temperatures as low as -20 ℃. The ultra-low hysteresis presented by the biomimetic hydrogel with ultra-low hysteresis makes it suitable for many engineering fields like electrical sensing with superior reliability (the corresponding electrical signal ($\Delta R/R_0$) is stable even after 1000 stretching-unstretching cycles). Moreover, the design strategy of hydrogels with programmable hysteresis provides an innovative methodology for the future development of smart high-performance hydrogels.

Keywords: double-network hydrogel; ultra-low hysteresis; electrical signal; freeze-resistance; smart materials

1. Introduction

Highly stretchable, tough and resilient elastomers and gels hold great importance in the fields of flexible electronics, wearable devices, biomedicine, and etc [1–5]. In practice, apart from high strength, stretchability, and toughness, low hysteresis over repeated loading–unloading cycles is critical for soft materials to ensure excellent resilience and resist fatigue [6–9].Owing to the poor mechanical robustness of single-network hydrogels—characterized by low strength, limited extensibility, and low fracture energy—researchers have engineered double-network (DN) hydrogels [10] that simultaneously achieve significantly improved toughness and stretchability [11–14]. Although the interpenetrating network (IPN) structure effectively suppresses crack propagation under mechanical loading, internal intermolecular friction leads to substantial energy dissipation, resulting in pronounced stress–strain hysteresis [15,16].The material exhibits fatigue behavior, as evidenced by a progressive decline in its mechanical properties under cyclic loading [17,18]. These phenomena primarily arise from—including intermolecular friction and irreversible rupture of internal bonds—in hydrogels subjected to cyclic loading [19–21]. Recently, great efforts have been made to reach low hysteresis (< 5%) upon cyclic tensile tests via supramolecular microstructures including multi-functional nano-crosslinkers, coiled protein/polypeptide and polypeptide/metal coordination [22–24]. In these cases, fast, efficient, and reversible disassembly/reassembly of supramolecular domains can significantly stabilize the internal microstructure and provide 'hidden

 doi:10.20944/preprints202605.0810.v1

length' to polymer networks under external stress—a feature that is highly beneficial for reducing intermolecular friction and hysteresis [25,26]. Moreover, the synergistic contribution of abundant non-covalent interactions and topological "hidden length" endows the hydrogel with remarkable stretchability and outstanding toughness [27].

However, "low hysteresis" is not an absolute intrinsic property of a material, but rather a condition-dependent, relative performance metric-strictly defined within specific loading–unloading protocols [28]. On one hand, it is typically observed under particular mechanical conditions, such as relatively high strain rates and moderate-to-low maximum strains. When the strain rate is reduced or the maximum strain is significantly increased, the hydrogel network gains sufficient time for viscoelastic relaxation and greater conformational reorganization space [29]. Under such conditions: (i) dynamic non-covalent crosslinks—including hydrogen bonds, coordination bonds, and boronate ester bonds—undergo progressive, multi-stage dissociation and reformation [30,31]; and (ii) polymer chains are prone to irreversible slippage or topological rearrangement (e.g. entanglement redistribution), thereby amplifying energy dissipation [32,33]. Consequently, the hysteresis ratio increases and residual strain accumulates—causing the material to deviate from the "low-hysteresis" regime [34,35]. On the other hand, the reported low hysteresis of hydrogels is normally recorded under mild conditions (i.e., ambient temperature). The anti-freezing or environmentally tolerant properties of hydrogels typically arise from the disruption of hydrogen bonding between water molecules—achieved [36] via high concentrations of hydrated ions, organic solvents, or hydrogen-bond-donating functional groups [37,38].However, these substances can introduce additional sacrificial bonds into the hydrogel network, thereby increasing intermolecular friction and hysteresis under cyclic loading [39]. Achieving low mechanical hysteresis in hydrogels under extreme environmental conditions remains a significant challenge.

The sarcomere—the fundamental contractile unit of striated muscle—exhibits exceptional adaptive mechanoresponsiveness to complex, dynamic mechanical loading [40]. Its hierarchical architecture, featuring aligned myofilaments and viscoelastic interfilamentary matrix, enables sustained high strength, toughness, and fatigue resistance [41] by minimizing intermolecular friction and preserving elastic recoil over repeated cycles [42–45]. Inspired by this, we developed a biomimetic double-network hydrogel (P-O-ALG-PA) comprising poly(acrylamide-co-octadecyl acrylate), sodium alginate, and phytic acid—integrated via synergistic covalent–ionic–hydrophobic crosslinking [46]. Unlike most reported high-strength and tough hydrogels, the mechanical behavior of P-O-ALG-PA arises from the synergistic interplay between supramolecular aggregates and interfacial lubrication.Remarkably, after a tailored preloading protocol, P-O-ALG-PA exhibits ultralow hysteresis (<0.02%) under cyclic tensile loading—even at low strain rates (~20 mm·min^{-1}) or large strains up to ~500%.Under high-speed, low-strain preloading, P-O-ALG-PA exhibits pronounced strain-stiffening behavior accompanied by negative hysteresis-suggesting an energy-releasing, self-reinforcing mechanism [47]. Furthermore, the programmable ultra-low hysteresis persists stably down to −20 °C. Its electrical sensing exhibits exceptional stability, fatigue resistance, and environmental robustness—enabling reliable operation in next-generation wearable electronics [48,49]. Moreover, P-O-ALG-PA exhibits autonomous self-healing, exceptional water retention, and robust, substrate-agnostic adhesion to diverse solid surfaces [50]. Collectively, this hydrogel achieves unprecedented environmental adaptability and programmable near-zero hysteresis, establishing a paradigm-shifting design strategy for hysteresis-free intelligent soft materials.

2. Results and Discussion

FTIR spectroscopy was employed to characterize the chemical structures of poly(octadecyl acrylate) (P-O), P-O–alginate (P-O-ALG), and P-O-ALG–phytic acid (P-O-ALG-PA) hydrogels (as Figure 1a shows). All samples exhibit a broad, intense band at 3200–3272 cm^{-1}, assigned to O–H stretching vibrations.A characteristic doublet appearing in the range of 2850–2926 cm^{-1} is assigned to the C–H stretching vibrations of –CH_2– and –CH_3 groups in the stearyl side chain, confirming the structural integrity of the poly(acrylate-18) main chain in all samples.In the 1438–1673 cm^{-1} region, a

 doi:10.20944/preprints202605.0810.v1

broad absorption band—assigned to the asymmetric stretching vibration of carboxylate (–COO^-) in sodium alginate and overlapped with H–O–H bending of bound water—exhibits progressive blue shifts: from 1590 cm^{-1} in P-O to 1660 cm^{-1} in P-O-ALG and finally to 1673 cm^{-1} in P-O-ALG-PA. This systematic shift reflects enhanced electron withdrawal and strengthened bonding due to coordinative interaction between –COO^- groups and phytic acid, corroborating progressive crosslinking and electronic modulation within the ternary network [51]. The band at 1431–1458 cm^{-1} is assigned to the symmetric COO^- stretching vibration, coupled with C–H in-plane bending, corroborating structural modulation induced by sodium alginate and phytic acid incorporation [52]. Notably, a strong, broad absorption band emerges exclusively in the P-O-ALG-PA spectrum within 1000–1200 cm^{-1}. This feature is assigned to overlapping P–O–C, P–O–H, and PO_4^{3-} stretching vibrations of phytic acid, together with C–O–C and C–O stretches from alginate's saccharide rings [53]. Its absence in P-O and P-O-ALG spectra confirms that phytic acid is not merely physically entrapped but is chemically integrated—via covalent bonding and/or coordination—into the hydrogel network, thereby establishing the ternary P-O-ALG-PA architecture.

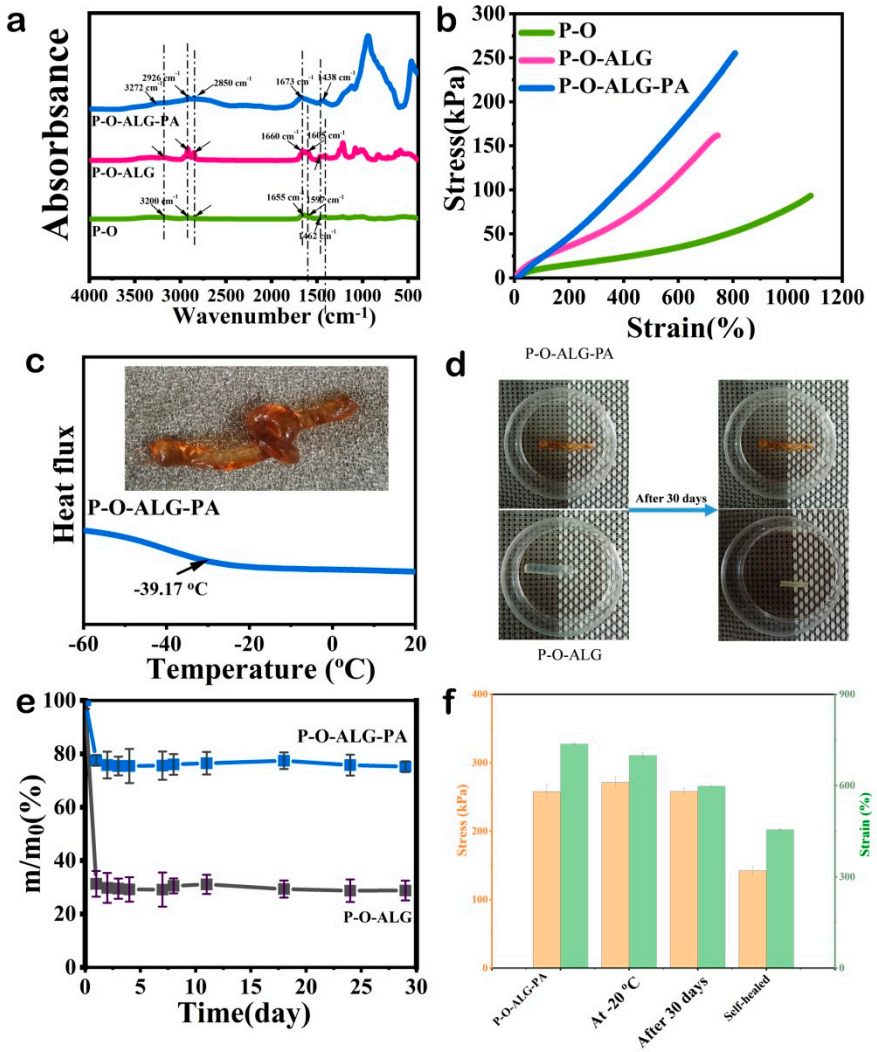

Figure 1. (a) FTIR spectra of the P-O-ALG-PA, P-O-ALG, P-O hydrogel. (b) Representative tensile curves of the tested hydrogels. (c) DSC curve of the P-O-SA-PA hydrogel from -60 ℃ to 20 ℃. The inset image shows that the hydrogel remains in a robust gel state at −20 °C and can be freely knotted without fracture. (d) Illustration of original P-O-SA-PA hydrogel, P-O-SA-PA hydrogel in the air after 30 days, the original P-O-SA hydrogel, and P-O-SA hydrogel in the air after 30 days. (e) Water-retaining capability and environmental durability of P-O-SA-PA and P-O-SA. (f) Corresponding stress-strain statistical data for the P-O-SA-PA hydrogel under the following

 doi:10.20944/preprints202605.0810.v1

conditions: as-prepared (room temperature), at −20 °C, after 30 days of ambient air storage at room temperature, and after self-healing following tensile damage.

As shown in Figure 1b, the mechanical strength of the sample increases significantly from P–O to P–O–ALG and further to P–O–ALG–PA, while the fracture strain remains at a relatively high level. This indicates that the incorporation of sodium alginate (ALG) and phytic acid (PA) effectively enhances the material's mechanical performance. To further explore the low-temperature conditions of P-O-ALG-PA hydrogel. As shown in Figure 1c, the DSC thermogram of the P-O-ALG-PA hydrogel reveals a glass transition temperature of −39.17 °C significantly below 0 °C enabling exceptional low-temperature elasticity and structural integrity [54,55]. This exceptionally low glass transition temperature serves as a key indicator of superior antifreezing performance, marking a significant advance in low-temperature-stable soft materials [56]. The outstanding antifreezing capability arises from the synergistic interplay among the three constituent components. Poly (octadecyl acrylate) (POA) acts as an intrinsic plasticizer, depressing the glass transition temperature and maintaining chain mobility at subzero temperatures. Its hydrophobic alkyl chains reduce unfrozen water content, thereby suppressing ice nucleation. ALG furnishes a robust polysaccharide scaffold that physically impedes ice-crystal propagation and preserves structural integrity. PA forms extensive hydrogen bonds with water molecules, restricting free-water mobility and inhibiting ice growth. Additionally, it serves as a multifunctional crosslinker, reinforcing the alginate network and enhancing mechanical stability under freezing conditions. This hierarchical synergy renders P-O-ALG-PA a promising candidate for low-temperature flexible electronics and implantable biomedical devices. Figure 1d shows that the P–O–ALG–PA hydrogel retains its elasticity after 30 days of storage at 25 °C and 30% relative humidity (RH), whereas the P–O–ALG control undergoes severe dehydration and embrittlement. Figure 1e quantitatively confirms that phytic acid (PA) forms strong hydrogen bonds with water molecules, effectively immobilizing them within the hydrogel network and thereby significantly suppressing water evaporation and loss. Statistical results of the tensile test in Figure 1f revealed that pristine P-O-ALG-PA hydrogel exhibits a high tensile strength of ~250 kPa and exceptional extensibility (~650% strain), demonstrating outstanding mechanical robustness and ductility. At −20 °C, the hydrogel retains a tensile stress of ~270 kPa and strain of ~600%, demonstrating exceptional low-temperature mechanical stability without embrittlement—consistent with its ultralow glass transition temperature (Tg = −39.17 °C) determined by DSC, confirming outstanding low temperature tolerance. After 30-day storage, tensile stress and strain remain within the same order of magnitude as the pristine hydrogel, confirming exceptional long-term stability. Notably, the hydrogel achieves ~60% recovery of both tensile stress (~150 kPa) and strain (~400%) after autonomous self-healing—without external stimuli—following mechanical rupture. This capability arises from reversible dynamic coordination bonds between phytic acid and oxidized alginate, enabling rapid bond reformation and restoration of structural integrity and mechanical functionality. These results demonstrate that P-O-ALG-PA hydrogel exhibits exceptional cryostability, long-term structural integrity, and autonomous self-healing—making it a promising candidate for flexible electronics, wearable sensors, and biomedical devices operating under harsh conditions.

Based on experimental evidence, the gelation mechanism is proposed as follows (Figure 2): Free-radical polymerization proceeds without chemical crosslinkers (e.g., MBA). SDS and NaCl synergistically stabilize the oil phase and enable uniform dispersion of OA [57]. Under APS initiation, OA self-assembles into nanoscale micelles—surfactant-stabilized by SDS hydrophilic heads which serve as dynamic physical crosslinking nodes, anchoring polyacrylamide (PAAm) chains into a robust primary network. Concurrently, sodium alginate constructs a secondary network via hydrogen bonding [6,20]. Subsequent dialysis removes residual SDS, followed by immersion in 70 wt% PA solution, enabling PA infiltration. PA's phosphate groups form reversible hydrogen bonds with alginate hydroxyls, reinforcing the dual-network architecture and endowing the hydrogel with enhanced mechanical integrity and stimuli-responsive dynamics.PA infiltration introduced

 doi:10.20944/preprints202605.0810.v1

abundant, reversible hydrogen bonds between its phosphate groups and hydroxyls of sodium alginate, serving as additional physical crosslinking points [58]. Concurrently, intra- and intermolecular hydrogen bonding among alginate hydroxyls drove hierarchical fibrillar alignment—morphologically and mechanically mimicking sarcomere—thereby significantly enhancing mechanical robustness.

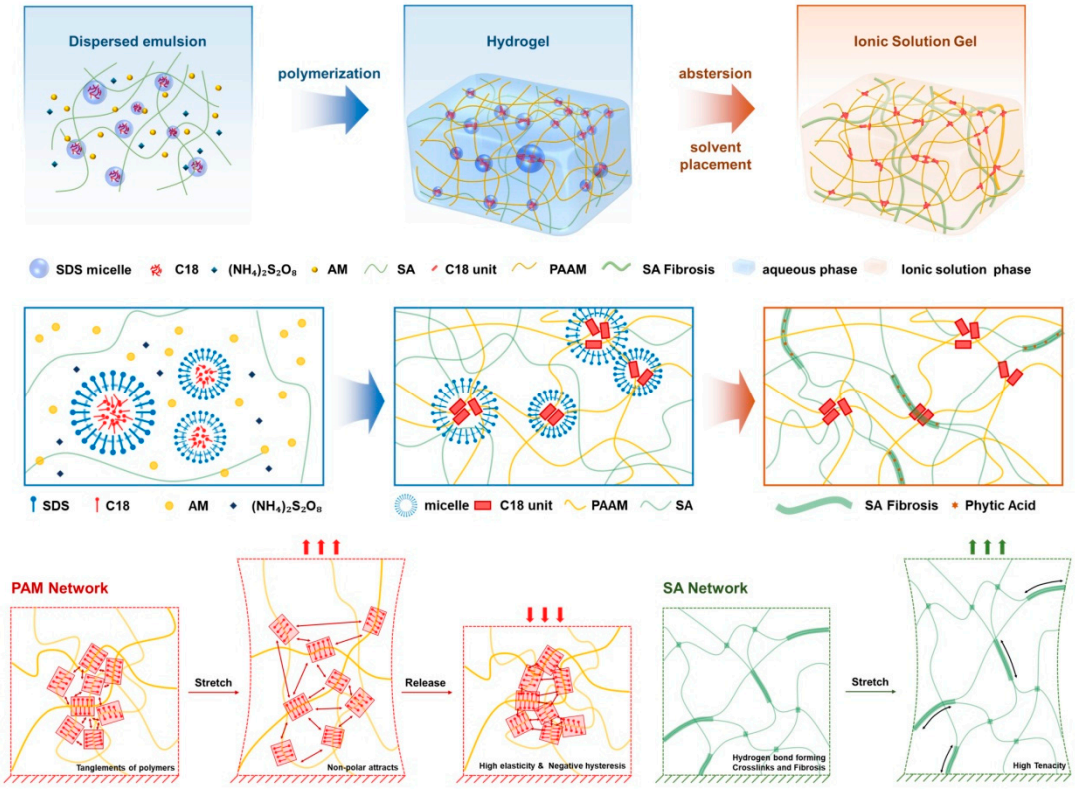

Figure 2. The fabrication procedure of the P-O-SA-PA hydrogel and representative structural schematics of the hydrogel at key synthesis stages.

Given its muscle-mimetic anisotropic microstructure, this hydrogel can biomimetically recapitulate the stretch–relaxation cycling behavior of skeletal muscle. Its fatigue behavior and biomimetic mechanical response are quantitatively characterized through the dynamic evolution of hysteresis ratio during cyclic loading–unloading tests. To systematically investigate the viscoelastic hysteresis and biomimetic muscular mechanical response of the P-O-SA-PA hydrogel, uniaxial cyclic tensile loading–unloading tests were performed using an universal testing machine. A dual-parameter experimental design was employed to probe the coupled effects of maximum strain (200%, 300%, 400%, and 500%) and strain rate (20, 50, 100, and 200 mm·min^{-1}).As shown in Figures S1 and 3a–c, we systematically investigated the cyclic loading–unloading behavior of the P-O-ALG-PA double-network hydrogel under combinatorial tensile strains (low/medium/high) and strain rates (high/medium/low). Strikingly, the hysteresis ratio (HR) is not a fixed parameter but exhibits programmable, condition-dependent modulation: HR peaks at <5% under high-strain–low-rate conditions; drops to ~0.2%—near-ideal elasticity—under medium-strain–medium-rate loading; and, most notably, attains a negative value of −8% under low-strain–high-rate conditions, unambiguously indicating net energy return (i.e., unloading work exceeds loading work). This negative HR, unprecedented for conventional hydrogels, is most pronounced in the first cycle and decays rapidly thereafter, reflecting a transient mechanical "training" or structural adaptation process intrinsic to the dynamic network. This dynamic hysteresis arises from phytic acid (PA)-induced "acid-induced precipitation" of sodium alginate (NaALG): PA's polyphosphate groups drive directional ALG chain

 doi:10.20944/preprints202605.0810.v1

rearrangement and fibrillation via robust hydrogen-bonding networks, yielding anisotropic, myofibril-mimetic microstructures. These confer multiple reversible energy-dissipation mechanisms—micelle dissociation/reassociation, hydrogen-bond scission/reformation, and fibrillar slippage—whose activation thresholds govern spatiotemporal matching with external mechanical stimuli, thereby directly determining hysteresis ratio (HR) magnitude and sign. We propose a biologically inspired "training-testing" framework for the tunable hysteresis behavior: high-strain/low-rate loading induces large HR, reflecting structural lag—akin to initial learning resistance; moderate strain/rate yields near-zero HR, signifying optimal stimulus–response synchronization and efficient energy transduction; low-strain/high-rate triggers negative HR, evidencing predictive energy storage/release—reminiscent of anticipatory task execution [59]. Crucially, this analogy is grounded in intrinsic dynamics of the PA-induced anisotropic fibrillar network: its orientational order, hydrogen-bond density, and hierarchical relaxation timescales collectively encode programmable "mechanical memory", enabling adaptive energy dissipation governed by spatiotemporal stimulus matching.

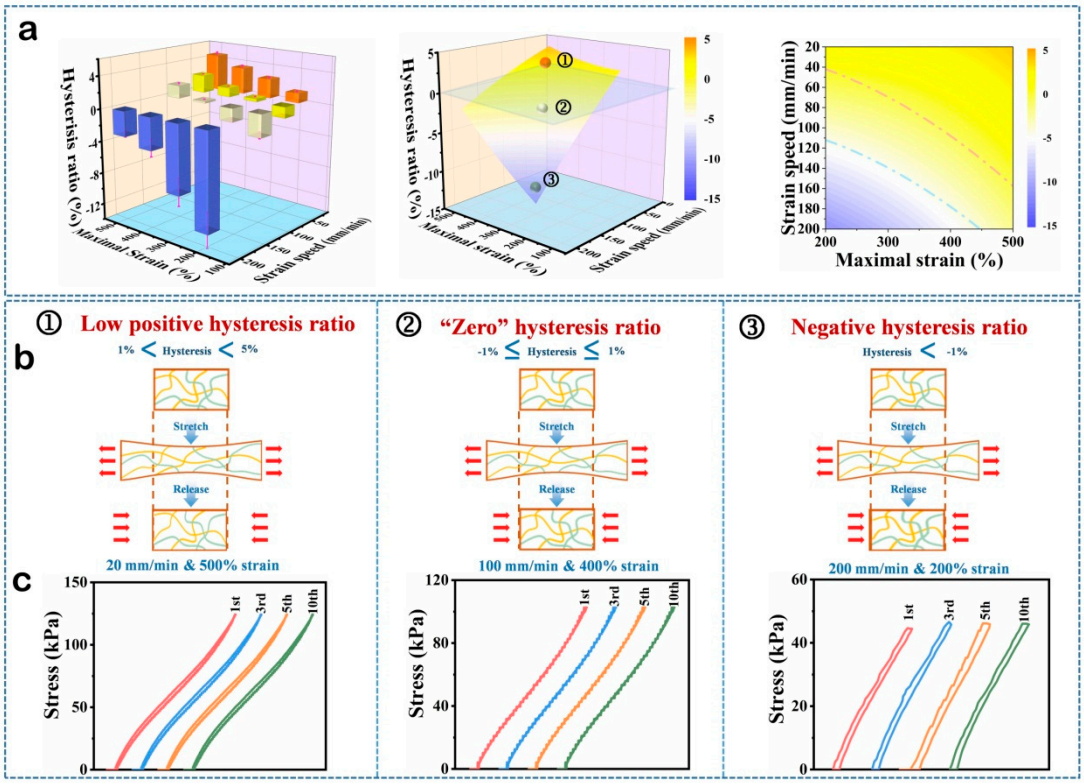

Figure 3. (a) Histograms of P-O-SA-PA at different stretching ratios and strain speeds. Three dimensional fitting surface corresponding with histograms. Corresponding phase image. (b) Schematic diagram of loading-unloading test. (c) Hysteresis loops of the hydrogel under tensile loading–unloading cycles at crosshead speeds of 20, 100, and 200 mm·min^{-1}, with corresponding maximum strains of 500%, 400%, and 200%, respectively.

This HR exhibits a systematic, load-condition–dependent tunability—representing a rare intrinsic programmable mechanical response. To elucidate its structural origin, we fabricated two control hydrogels: P-B-AlG-PA (crosslinked with MBA instead of stearyl acrylate, lacking hydrophobic moieties) and P-O-PA (devoid of alginate but retaining phytic acid and hydrophobic components). Notably, complete omission of OA prevents gelation, confirming its dual role as both covalent crosslinker and hydrophobic microdomain builder. Under identical coupled stretch-ratio/strain-rate cycling protocols, P-B-AlG-PA yields a high, invariant HR (~20% in Figure S2), devoid of rate- or amplitude-dependence (Figure 4a). In Figure 4b, the large enclosed area of the loading–unloading curves for ①and ② verifies the high hysteresis rate of P-B-AlG-PA. This loss of

 doi:10.20944/preprints202605.0810.v1

programmability unambiguously identifies the dynamic hydrophobic association network—derived from OA—as the essential structural motif enabling programmable HR regulation.

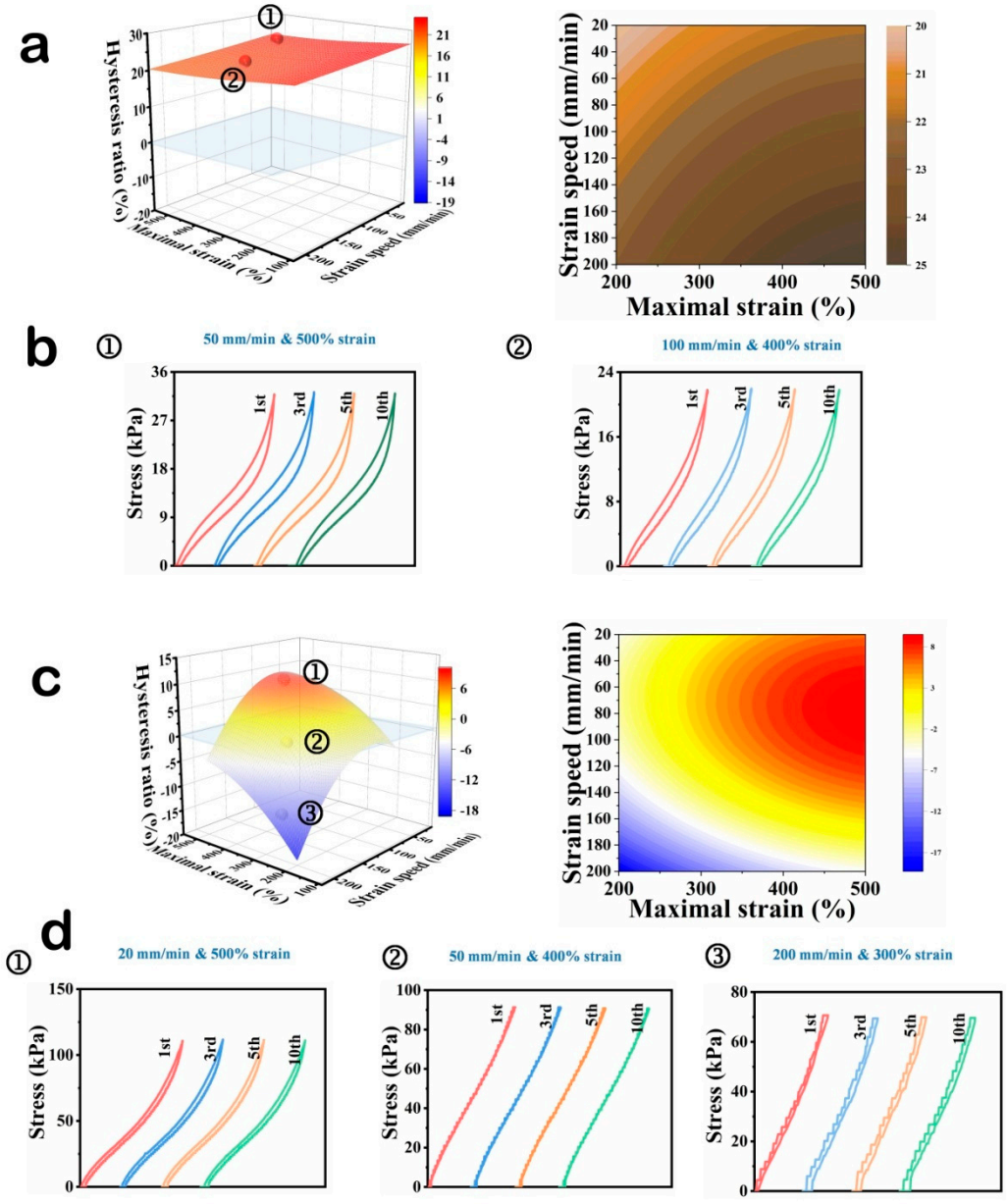

Figure 4. (a) Three dimensional surface graph of P-B-SA-PA hydrogel. Corresponding phase image. (b) Hysteresis loops of the hydrogel under tensile loading–unloading cycles at crosshead speeds of 50 and 100 mm·min^{-1}, with corresponding maximum strains of 500%, and 400%, respectively. (c) Three dimensional surface graph of P-O-PA hydrogel. Corresponding phase image. (d) Hysteresis loops of the hydrogel under tensile loading–unloading cycles at crosshead speeds of 20, 50 and 200 mm·min^{-1}, with corresponding maximum strains of 500%, and 400%, and 300%, respectively.

Cyclic loading–unloading tests of P-O-PA under identical strain-amplitude and strain-rate coupling conditions (Figures S3 and 4c,d) reveal retained rate- and amplitude-dependent hysteresis, yet HR increases markedly (−20% to +10%). This elevation stems directly from the absence of sodium alginate (AlG). AlG synergizes with phytic acid (PA) via directional hydrogen bonding to drive hierarchical nanofibril bundle assembly, establishing a reversible energy-dissipation pathway. In contrast, P-O-PA lacks this structural motif; its sole dissipative network—comprising hydrophobic associations and phosphate–hydrogen bonds between stearyl acrylate and PA—exhibits elevated

 doi:10.20944/preprints202605.0810.v1

dissociation energy barriers and sluggish reassociation kinetics, thereby amplifying irreversible interfacial friction and systematically elevating HR. Collectively, these results confirm that the programmable, low-hysteresis mechanical response of P-O-ALG-PA arises exclusively from the precise integration of four components: AM (monomer), OA (dual-function crosslinker/hydrophobe), ALG, and PA, each indispensable to the designed dual-network architecture.

To systematically validate the programmable "training–testing" response of the hydrogel, we performed coupled experiments: controlled mechanical preconditioning (termed "training") followed by subsequent mechanical testing (termed "testing"), as schematically illustrated in Figure 5a. A high-intensity training protocol—10 cycles of uniaxial stretching to 500% engineering strain at 100 mm·min^{-1}—was applied first. Subsequently, stepwise strain-controlled testing was performed at the same crosshead speed (100 mm·min^{-1}), using progressively decreasing engineering strain levels: 400%, 300%, and 200%. As shown in Figure 5b, the hysteresis ratio (HR) decreased markedly and fell below 2.5%, indicating that intense mechanical preconditioning drives structural reorganization within the dual network, thereby enhancing the reversibility of energy dissipation [60]. Further, we implemented a training–testing protocol in which the training speed exceeded the testing speed to probe the variation of HR as Figure 5c shows. High-intensity "training" (300% strain, 200 mm·min^{-1}, 10 cycles) induced HR to −9% (Figure 5d), indicating dynamic bond reconfiguration exceeding instantaneous energy dissipation—i.e., "overfitting." Subsequent "examination" under milder conditions (200% strain, 100 mm·min^{-1}) yielded stable HR < 2.5%, demonstrating that overtraining confers broad mechanical adaptability.

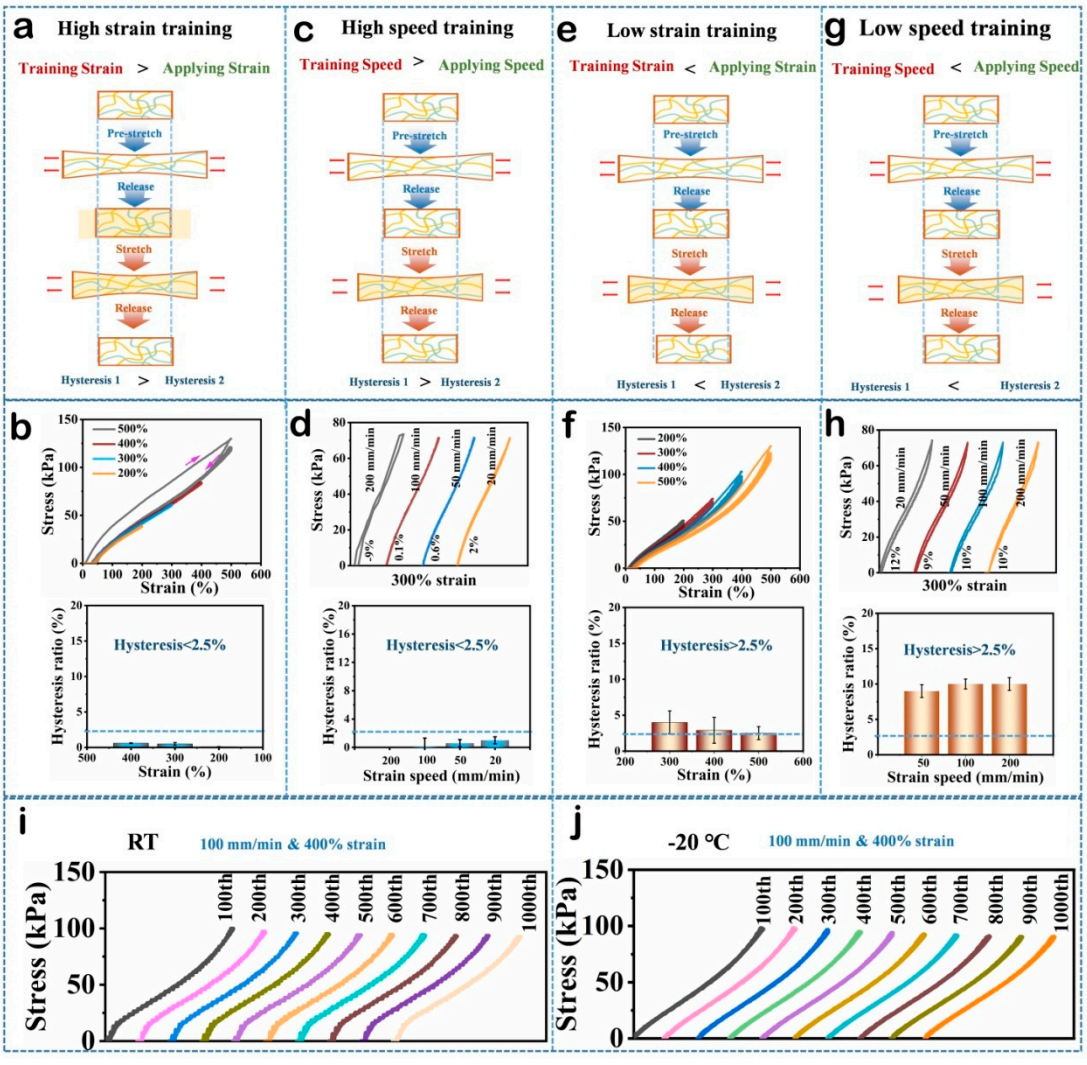

Figure 5. (a) Schematic illustration of the "High-Magnification Learning-Low-Magnification Assessment" paradigm of the P-O-SA-PA hydrogel. (b) Loading-unloading curves at 100 mm/min from the strain of 500% to

 doi:10.20944/preprints202605.0810.v1

200%, and hysteresis ratio responds to each applying strain. (c) High speed training mode of the P-O-SA-PA hydrogel. (d) Loading-unloading curves at a strain of 300% from stretching speed of 200 to 20 mm/min. and hysteresis ratio responds to the applying strain. (e) Low strain training behavior. (f) Loading-unloading curves at 100 mm/min from the strain of 200% to 500%, and hysteresis ratio responds to the applying strain. (g) Low strain training behavior. (h) Loading-unloading curves at a strain of 300% from stretching speed of 20 to 200 mm/min, and hysteresis ratio responds to the applying strain. (i) 1000 cycles of stretching-unstretching curves at room temperature. (j) Anti-fatigue measurements at -20 ℃.

Conversely, when the training strain (200%) is lower than the subsequent test strain (from 300% to500%, Figure 5e), the hysteresis ratio (HR) remains elevated (> 2.5%) and fails to reach the low values (<2.5%) achieved under matched-strain conditions (Figure 5f). Each stepwise increase in test strain therefore requires one additional preconditioning cycle at that strain level to restore a low HR—revealing that HR is dependent on the learning pattern. The low-rate training mode exhibits the same behavior such as Figure 5g,h show.

This training–testing paradigm not only demonstrates precise programmability of the hysteresis ratio (HR) through predefined mechanical protocols but also reveals its mechanistic origin: synergistic reorganization of hydrophobic association domains and hydrogen-bonding networks within the dual-crosslinked architecture. Under 400% engineering strain, 100 mm·min^{-1} crosshead speed, and 25 °C, HR remains stable at 0.20 ± 0.02% over 1000 cycles (Figure 5i), with no measurable degradation in tensile modulus, elongation at break, or elastic recovery. Crucially, this exceptional fatigue resistance is fully retained at −20 °C (Figure 5j), indicating that the hydrogel retains its dynamic activity even at subzero temperatures. Collectively, P-O-AlG-PA hydrogel exhibits mechanically programmable low-hysteresis behavior, establishing a robust material platform for high-fidelity cyclic operation, including real-time soft strain sensing and reversible biomimetic actuation.

This low-hysteresis, programmable hydrogel markedly extends the performance frontier of flexible strain sensors. Its tunable hysteresis—rooted in a “training–examination” dynamic bond regulation mechanism—effectively suppresses signal drift and response lag arising from viscous energy dissipation in conventional hydrogels, enabling high-fidelity, and highly reproducible strain-to-electrical transduction [61]. In human joint motion tests (wrist, elbow, knee bent synchronously to 90° in Figure 6a–c), site-specific signal amplitudes are clearly resolved, with negligible phase lag and no amplitude decay. Robust wide-temperature responsiveness is further confirmed by finger flexion across angles at both 25 °C and −20 °C (Figure 6d,e). Under rigorous cyclic loading (400% strain, 100 mm·min^{-1}, 1000 cycles) such as Figure 6f shows, the hydrogel maintains a constant hysteresis of 0.2% and stable, non-drifting conductivity a direct consequence of synergistic dual-network rearrangement kinetics. This behavior is also retained under long-term cyclic loading at −20 °C (Figure 6g).These attributes confer exceptional large-strain adaptability, cryo-stability, and operational longevity. This stems from the “learning–examination” system-enabled hysteresis tunability, ensuring faithful transduction of dynamic motion trajectories with robust large-strain adaptability, cryo-stability (−20 °C), and fatigue-resistant signal fidelity—enabling high-precision human motion monitoring, extreme-environment flexible electronics, and closed-loop biofeedback systems.

 doi:10.20944/preprints202605.0810.v1

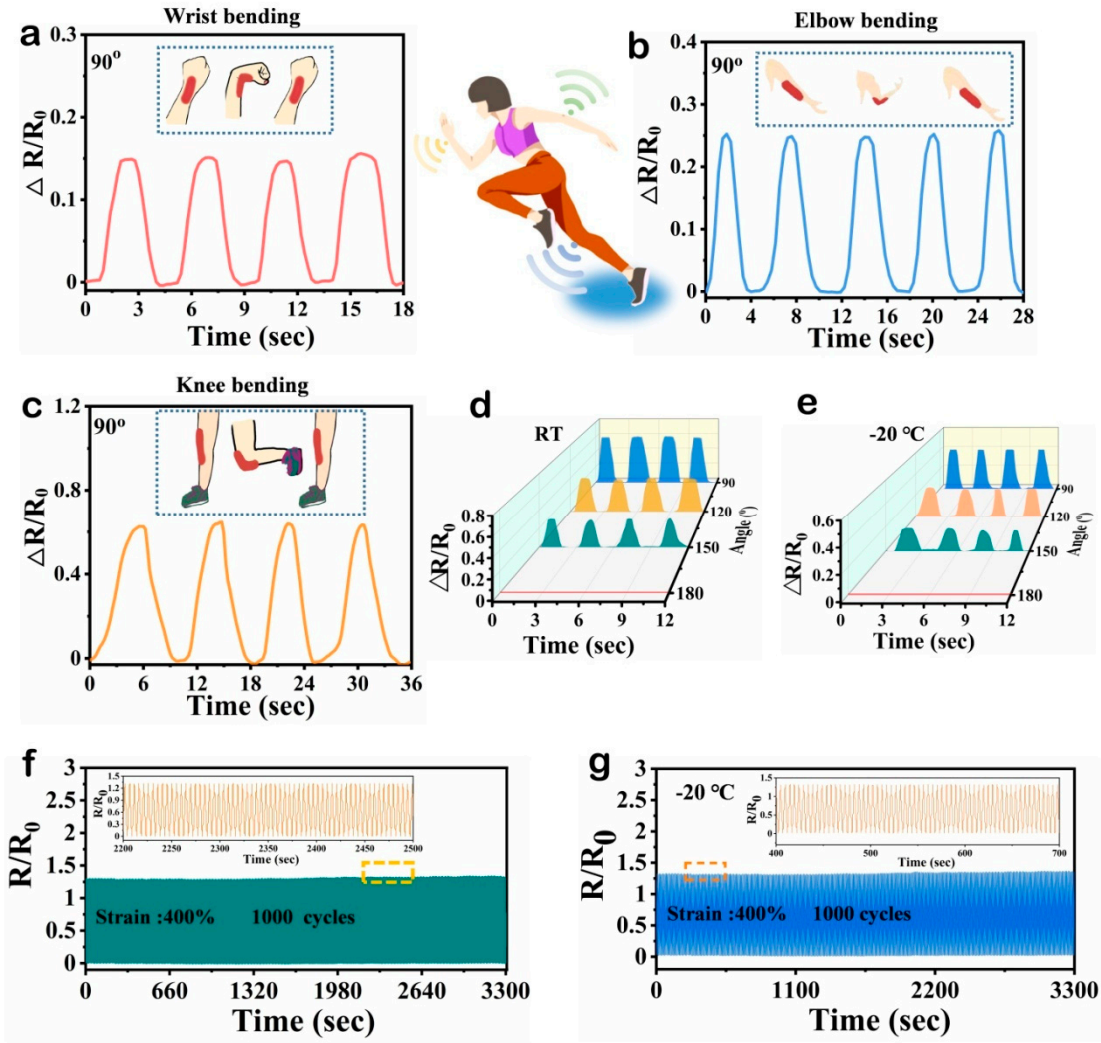

Figure 6. Strain-dependent electrical response of the P-O-SA-PA hydrogel sensor mounted on (a) the wrist, (b) the elbow, and (c) the knee, each bent to 90°. Robust wide-temperature responsiveness is further confirmed by knee flexion across angles at both (d) 25 °C and (e) −20 °C. Long-term (3.3×10^3 s) electromechanical response of the P-O-SA-PA hydrogel was recorded under cyclic loading–unloading protocols using a universal testing machine at both (f) room temperature and (g) −20 °C.

3. Conclusions

In summary, we report a chemically unmodified, physically crosslinked hydrogel comprising PAM, OA, ALG, and PA. This material exhibits exceptional antifreezing capability (down to −20 °C), autonomous self-healing, ultralow and programmable hysteresis (hysteresis rate fixed at 0.2% after 1000 cycles), and stable conductivity. It delivers high-fidelity, non-hysteretic, drift-free electromechanical transduction during dynamic joint motions (wrist, elbow, knee, fingers) across a broad temperature range. These integrated properties—originating from synergistic dual-network reconfiguration kinetics and the "training–testing" hysteresis programming strategy—establish it as a robust, mechanism-guided sensing matrix for high-precision wearable motion monitoring and extreme-environment flexible electronics.

 doi:10.20944/preprints202605.0810.v1

4. Experimental

4.1. Materials

Acrylamide (AM) was used as monomer to form primary network copolymerized with oil-soluble monomers octadecyl acrylate (OA). Sodium chloride (NaCl) and sodium dodecyl sulfate (SDS) were used as solubilizing agents to enhance the aqueous dispersibility and surface wetting of C18-functionalized materials. Sodium alginate (ALG) was employed as the secondary network component. Ammonium persulfate (APS) was chosen as initiator. Phytic acid (PA)70% (w/w, aqueous solution) was used as a solution to soak the achieved sample. All reagents in this work were used aspurchased from Aladdin Reagent Inc. without further purification.

4.2. Hydrogel Preparation

In order to obtain the ALG oleogel, the operation steps are as follows: ALG (0.15 g) was dissolved in 5 mL of deionized water under continuous magnetic stirring at room temperature until a homogeneous, viscous solution was obtained. Subsequently, 0.9 g AM was added and uniformly dispersed. Under a water bath temperature of 50 °C, OA, SDS, and NaCl were sequentially added to the aqueous phase at mass fractions of 14%, 35%, and 25% (w/w), respectively, based on the total mass of solutes [62]. SDS micelles enabled effective solubilization and nanoscale dispersion of OA, establishing a microscopically heterogeneous polymerization medium. APS was then added as a thermal initiator, and the mixture was homogenized. The resulting precursor solution was sealed in a polypropylene tube and polymerized thermally at 45 °C to afford the ALG-based organogel precursor.

SDS in the SA-based organogel impairs both optical clarity and mechanical robustness. To eliminate SDS completely, the organogel underwent exhaustive dialysis against deionized water until constant weight was achieved, followed by solvent exchange—replacing the aqueous phase with a 70 wt% PA solution for 7 h. This protocol yielded a homogeneous, optically transparent, brownish, and flexible P-O-ALG-PA organogel.

For comparation, oleogel without ALG, ALG oleogel without soaking in PA, swelled oleogel, swelled ALG oleogel, oleogel soaked in PA are prepared for future use.

4.3. Characterizations

Fourier transform infrared spectroscopy (FTIR) was carried out on a Spectrum 100 spectrophotometer (PerkinElmer) with wavenumbers ranging from 4000 to 600 cm^{-1}, with a resolution of 1 cm^{-1}. Differential scanning calorimetry (DSC) was conducted on a Q2000 differential scanning calorimeter (TA instruments) by using the as-prepared organogel, the sample within the temperature ranging from −90 to 80°C. The scan rate was set to be 5 °C min^{-1}, and the nitrogen flow rate was 20 mL min^{-1}.

4.4. Tensile Testing

A universal tensile testing machine (STS10K model, Xiamen East Instrument Co., Ltd.) was used to evaluate the mechanical properties of the as-prepared samples. Tests were conducted with a maximum applied load of 20 N. A constant crosshead speed of 100 mm·min^{-1} was employed for all tensile tests. At least five replicate specimens were tested to ensure statistical reliability, and control samples were tested in parallel under identical conditions.

4.5. Hysteresis Testing

The hysteresis properties of the samples were measured on the same machine.At a constant strain rate of 100 mm·min^{-1}, we systematically investigated the path-dependent hysteresis (500%→100% vs. 100%→500%) of the hydrogel. Concurrently, at a fixed tensile strain of 300%, we quantified the strain-rate dependence of hysteresis over the range 20–200 mm·min^{-1}.This dual-

 doi:10.20944/preprints202605.0810.v1

parameter–dependent hysteresis constitutes a programmable, learning-test–mimetic mechanical system.

4.6. Electrical Test

The deformation of P-O-ALG-PA organogel corresponds to the change in the resistance of the hydrogel, the function relationship can be established to realize strain sensing. The conductivity (σ, Sm^{-1}) of the observed sample can be confirmed by CHI 760E electrochemical workstation. The conductivity is calculated by the following formula:

$\sigma = L/(R \times A)$

L (in m), A (in m^2), and R (in Ω) denote the distance between adjacent electrodes, the cross-sectional area of the hydrogel, and its electrical resistance, respectively.

The oleogel can be attached to wrist, elbow or knee of the volunteer and act as a sensor which connects with CHI 760E electrochemical workstation. With the aid of tensile testing machine, long cycles of testing can be carried out. The electric signal can be recorded following the cycled stretching by the tensile testing machine.

The following formula was used to calculate the variation of resistance:

$\triangle R/R_0 = (R-R_0)/R_0 \times 100\%$

where R_0 and R represent the resistance of the original hydrogel and stretching hydrogel, respectively.

Supplementary Materials: The following supporting information can be downloaded at the website of this paper posted on Preprints.org.

Acknowledgments: This work was supported by Fundamental Research Funds for the Central University No. 9161023009.

References

1. Singh A. K.; Sarkar D; Khan G. G.; Mandal K. Hydrogenated NiO nanoblock architecture for high performance pseudocapacitor. ACS Appl. Mater. Interfaces. **2014**, 6, 4684-4692.
2. Raffa P; Easler M; Urciuolo A. Three-dimensional in vitro models of neuromuscular tissue. Neural Regener. Res. **2022**, 17, 759-66.
3. Ge G; Lu Y; Qu X; Zhao W; Ren Y; Wang W; Wang Q; Huang W; Dong X. Muscle-Inspired Self-Healing Hydrogels for Strain and Temperature Sensor. ACS nano. **2020**, 14, 218-228.
4. Liang X; Chen G; Lin S; Zhang J; Wang L; Zhang P; Wang Z; Wang Z; Lan Y; Ge Q; Liu J. Anisotropically Fatigue-Resistant Hydrogels. Adv. Mater. **2021**, 33, e2102011.
5. Thakur N; Chaudhary A; Chakraborty A; Kumar R; Sarma T. K. Ion Conductive Phytic Acid-G Quadruplex Hydrogel as Electrolyte for Flexible Electrochromic Device. Chem Nano Mat. **2021**, 7, 613-619.
6. Wang A; Wang Y; Zhang B; Wan K; Zhu J; Xu J; Zhang C; Liu T. Hydrogen-bonded network enables semi-interpenetrating ionic conductive hydrogels with high stretchability and excellent fatigue resistance for capacitive/resistive bimodal sensors. Chem. Eng. J. **2021**, 411, 128506.
7. Li Y; Wang D; Wen J; Liu J; Zhang D; Li J; Chu H. Ultra-Stretchable, Variable Modulus, Shape Memory Multi-Purpose Low Hysteresis Hydrogel Derived from Solvent-Induced Dynamic Micelle Sea-Island Structure. Adv. Funct. Mater. **2021**, 31, 2011259.
8. Feng E; Li J; Zheng G; Li X; Wei J; Wu Z; Ma X; Yang Z. Mechanically toughened conductive hydrogels with shape memory behavior toward self-healable, multi-environmental tolerant and bidirectional sensors. Chem. Eng. J. **2022**, 432, 134406.
9. Duan J; Liang X; Guo J; Zhu K; Zhang L. Ultra-Stretchable and Force-Sensitive Hydrogels Reinforced with Chitosan Microspheres Embedded in Polymer Networks. Adv. Mater. **2016**, 28, 8037-8044.
10. Huang Q; Cai Y; Zhang X; Liu J; Liu Z; Li B; Wong H; Xu F; Sheng L; Sun D; Qin J; Luo Z; Lu X. Aligned Graphene Mesh-Supported Double Network Natural Hydrogel Conduit Loaded with Netrin-1 for Peripheral Nerve Regeneration. ACS Appl. Mater. Interfaces. **2021**, 13, 112-122.

 doi:10.20944/preprints202605.0810.v1

11. Revathi D; Panda S; Deshmukh K; Khotele N; Murthy V. R. K; Pasha S. K. K. Smart hydrogels for sensing and biosensing-Preparation, smart behaviours, and emerging applications- A comprehensive review. Polym. Test. **2025**, 150, 108912.
12. Fu R; Guan Y; Xiao C; Fan L; Wang Z; Li Y; Yu P; Tu L; Tan G; Zhai J; Zhou L; Ning C. Tough and Highly Efficient Underwater Self-Repairing Hydrogels for Soft Electronics. Small Methods. **2022**, 6, e2101513.
13. Zhang W; Liu X; Wang J; Tang J; Hu J; Lu T; Suo Z. Fatigue of double-network hydrogels. Eng. Fract. Mech. **2018**, 187, 74-93.
14. Gong Z; Zhang G; Zeng X; Li J; Li G; Huang W; Sun R; Wong C. High-Strength, Tough, Fatigue Resistant, and Self-Healing Hydrogel Based on Dual Physically Cross-Linked Network. ACS Appl. Mater. Interfaces. **2016**, 8, 24030-24037.
15. Das S; Martin P; Vasilyev G; Nandi R; Amdursky N; Zussman E. Processable, Ion-Conducting Hydrogel for Flexible Electronic Devices with Self-Healing Capability. Macromolecules. **2020**, 53, 11130-11141.
16. Zhang Y; Liao J; Wang T; Sun W; Tong Z. Polyampholyte Hydrogels with pH Modulated Shape Memory and Spontaneous Actuation. Adv. Funct. Mater. **2018**, 28, 1707245.
17. Heo J. W.; Yoo S. Z.; No M. H.; Park D. H.; Kang J. H.; Kim T. W.; Kim C. J.; Seo D. Y.; Han J; Yoon J. H.; Jung S. J.; Kwak H. B. Exercise Training Attenuates Obesity-Induced Skeletal Muscle Remodeling and Mitochondria-Mediated Apoptosis in the Skeletal Muscle. Int. J. Environ. Res. Public Health. **2018**, 15, 2301.
18. Xue B; Bashir Z; Guo Y; Yu W; Sun W; Li Y; Zhang Y; Qin M; Wang W; Cao Y. Strong, tough, rapid-recovery, and fatigue-resistant hydrogels made of picot peptide fibres. Nat. Commun. **2023**, 14, 2583.
19. Zhang S; Ren D; Zhao Q; Peng M; Wang X; Zhang Z; Liu W; Huang F. Observation of topological hydrogen-bonding domains in physical hydrogel for excellent self-healing and elasticity. Nat. Commun. **2025**, 16, 2371.
20. Liu X; Zhang Q; Gao G. Solvent-Resistant and Nonswellable Hydrogel Conductor toward Mechanical Perception in Diverse Liquid Media. ACS nano. **2020**, 14, 13709-13717.
21. Li J; Ding Q; Wang H; Wu Z; Gui X; Li C; Hu N; Tao K; Wu J. Engineering Smart Composite Hydrogels for Wearable Disease Monitoring. Nano-micro Lett. **2023**, 15, 105.
22. Wang Y, Xie Y, Xie X, Wu D, Wu H, Luo X, Wu Q, Zhao L, Wu J. Compliant and Robust Tissue-Like Hydrogels via Ferric Ion-Induced of Hierarchical Structure. Advanced Functional Materials. **2023**, 33, 2210224.
23. Suneetha M; Sun M. O; Mo C. S; Zo S; Madhusudana R. K; Soo H. S. Tissue-adhesive, stretchable, and self-healable hydrogels based on carboxymethyl cellulose-dopamine/PEDOT:PSS via mussel-inspired chemistry for bioelectronic applications. Chem. Eng. J. **2021**, 426, 130847.
24. Bai R; Yang J; Morelle X. P.; Yang C; Suo Z. Fatigue Fracture of Self-Recovery Hydrogels. ACS Macro Lett. **2018**, 7, 312-317.
25. Di X; Li J; Yang M; Zhao Q; Wu G; Sun P. Bioinspired, nucleobase-driven, highly resilient, and fast-responsive antifreeze ionic conductive hydrogels for durable pressure and strain sensors. J. Mater. Chem. A. **2021**, 9, 20703-20713.
26. Zhang G; Chen S; Peng Z; Shi W; Liu Z; Shi H; Luo K; Wei G; Mo H; Li B; Liu L. Topologically Enhanced Dual-Network Hydrogels with Rapid Recovery for Low-Hysteresis, Self-Adhesive Epidemic Electronics. ACS Appl. Mater. Interfaces. **2021**, 13, 12531-12540.
27. Matsumoto M; Water Driven Soft Actuator. Appl. Syst. Innov. **2018**, 1, 41.
28. Sun X; Luo F; Jiang F. Low-Hysteresis Cellulose-Based Hydrogels for Strain Detecting. Macromol. Rapid Commun. **2025**, 0, e00521.
29. Chang Q; He Y; Liu Y; Zhong W; Wang Q; Lu F; Xing M. Protein Gel Phase Transition: Toward Superiorly Transparent and Hysteresis-Free Wearable Electronics. Adv. Funct. Mater. **2020**, 30, 1910080.
30. Gao Y; Gu S; Jia F; Gao G. A skin-matchable, recyclable and biofriendly strain sensor based on a hydrolyzed keratin-containing hydrogel. J. Mater. Chem. A. **2020**, 8, 24175-24183.
31. Dai L; Wang Y; Li Z; Wang X; Duan C; Zhao W; Xiong C; Nie S; Xu Y; Ni Y. A multifunctional self-crosslinked chitosan/cationic guar gum composite hydrogel and its versatile uses in phosphate-containing water treatment and energy storage. Carbohydr Polym. **2020**, 244, 116472.

 doi:10.20944/preprints202605.0810.v1

32. Liu T; Ren X; Zhang J; Liu J; Ou R; Guo C; Yu X; Wang Q; Liu Z. Highly compressible lignin hydrogel electrolytes via double-crosslinked strategy for superior foldable supercapacitors. J. Power Sources. **2020**, 449, 227532.
33. Yang T; Xie P; Wu Z; Liao Y; Chen W; Hao Z; Wang Y; Zhu Z; Teng W. The Injectable Woven Bone-Like Hydrogel to Perform Alveolar Ridge Preservation With Adapted Remodeling Performance After Tooth Extraction. Front. bioeng. biotechnol. **2020**, 8, 119.
34. Bellinger P; Bourne M. N.; Duhig S; Lievens E; Kennedy B; Martin A; Cooper C; Tredrea M; Rice H; Derave W; Minahan C. Relationships between Lower Limb Muscle Characteristics and Force-Velocity Profiles Derived during Sprinting and Jumping. Med. Sci. Sport Exer. **2021**, 53, 1400-1411.
35. Xu K; Shen K; Yu J; Yang Y; Wei Y; Lin P; Zhang Q; Xiao C; Zhang Y; Cheng Y. Ultradurable Noncovalent Cross-Linked Hydrogels with Low Hysteresis and Robust Elasticity for Flexible Electronics. Chem. Mater. **2022**, 34, 3311-3322.
36. Liu W; Song M. S.; Kong B; Cui Y. Flexible and Stretchable Energy Storage: Recent Advances and Future Perspectives. Adv. Mater. **2017**, 29, 1603436.
37. Zhang Z; Qin C; Feng H; Xiang Y; Yu B; Pei X; Ma Y; Zhou F. Design of large-span stick-slip freely switchable hydrogels via dynamic multiscale contact synergy. Nat. Commun. **2022**, 13, 6964.
38. Chen G; Huang J; Gu J; Peng S; Xiang X; Chen K; Yang X; Guan L; Jiang X; Hou L. Highly tough supramolecular double network hydrogel electrolytes for an artificial flexible and low-temperature tolerant sensor. J. Mater. Chem. A. **2020**, 8, 6776-6784.
39. Yang C; Suo Z. Hydrogel ionotronics. Nat. Rev. Mater. **2018**, 3, 125-142.
40. Hu N; Zhang L; Yang C; Zhao J; Yang Z; Wei H; Liao H; Feng Z; Fisher A; Zhang Y; Xu Z. J. Three-dimensional skeleton networks of graphene wrapped polyaniline nanofibers: an excellent structure for high-performance flexible solid-state supercapacitors. Sci. Rep. **2016**, 6, 19777.
41. Chen M; Ren X; Dong L; Li X; Cheng H. Preparation of dynamic covalently crosslinking keratin hydrogels based on thiol/disulfide bonds exchange strategy. Int. J. Biol. Macromol. **2021**, 182, 1259-1267.
42. Gao L; Zhou Y; Peng J; Xu C; Xu Q; Xing M; Chang J. A novel dual-adhesive and bioactive hydrogel activated by bioglass for wound healing. NPG Asia Mater. **2019**,11, 66.
43. Li Y; Poon C. T.; Li M; Lu T. J.; Pingguan-Murphy B; Xu F. Chinese-Noodle-Inspired Muscle Myofiber Fabrication. Adv. Funct. Mater. **2015**, 25,5999-6008.
44. Joanisse S; Snijders T; Nederveen J. P.; Parise G. The Impact of Aerobic Exercise on the Muscle Stem Cell Response. Exerc. Sport Sci. Rev. **2018**, 46, 180-187.
45. Carleton M. M; Locke M; Sefton M. V. Methacrylic acid-based hydrogels enhance skeletal muscle regeneration after volumetric muscle loss in mice. Biomaterials. **2021**, 275, 120909.
46. Awasthi S; Gaur J. K; Pandey S. K.; Bobji M. S.; Srivastava C. High-Strength, Strongly Bonded Nanocomposite Hydrogels for Cartilage Repair. ACS Appl. Mater. Interfaces. **2021**, 13, 24505-24523.
47. Ibata N; Terentjev E. M. Why exercise builds muscles: titin mechanosensing controls skeletal muscle growth under load. Biophys. J. **2021**, 120, 3649-3663.
48. Balan E; Diman A; Everard A; Nielens H; Decottignies A; Deldicque L. Endurance training alleviates MCP-1 and TERRA accumulation at old age in human skeletal muscle. Exp. Gerontol. **2021**, 153, 111510.
49. Okada M; Nakai A; Hara E. S.; Taguchi T; Nakano T; Matsumoto T. Biocompatible nanostructured solid adhesives for biological soft tissues. Acta Biomater.. **2017**, 57, 404-413.
50. Lu X; Si Y; Zhang S; Yu J; Ding B. In Situ Synthesis of Mechanically Robust, Transparent Nanofiber-Reinforced Hydrogels for Highly Sensitive Multiple Sensing. Adv. Funct. Mater. **2021**, 31, 2103117.
51. Yang M; Zhao S; Zhao C; Cui J; Wang Y; Fang X; Zheng J. Caseinate-reinforced pectin hydrogels: Efficient encapsulation, desirable release, and chemical stabilization of (-)-epigallocatechin. International journal of biological macromolecules. **2023**, 230, 123298.
52. Song L; Wang Z; Chen S; Shen Y; Yin J; Wang R. Phytic Acid-Induced Gradient Hydrogels for Highly Sensitive and Broad Range Pressure Sensing. Adv. Mater. **2025**, 37, e2417978.
53. Zeng L; Liu B; Gao G. Physically crosslinked polyvinyl alcohol/chitosan-phytic acid hydrogels for wearable sensors with highly conductive, recyclable and antibacterial properties. Sci. China Mater. **2023**, 66, 4062-4070.

 doi:10.20944/preprints202605.0810.v1

54. Cai J; He Y; Zhou Y; Yu H; Luo B; Liu M. Polyethylene glycol grafted chitin nanocrystals enhanced, stretchable, freezing-tolerant ionic conductive organohydrogel for strain sensors. Compos. Part A: Appl. S. **2022**, 155, 106813.
55. Desnos H; Baudot A; Teixeira M; Louis G; Commin L; Buff S; Bruyère P. Ice induction in DSC experiments with Snomax®. Thermochimica Acta. **2018**, 667, 193-206.
56. Tan P; Wang H; Xiao F; Lu X; Shang W; Deng X; Song H; Xu Z; Cao J; Gan T; Wang B; Zhou X. Solution-processable, soft, self-adhesive, and conductive polymer composites for soft electronics. Nat. Commun. **2022**, 13, 358.
57. Gulyuz U; Okay O. Self-healing polyacrylic acid hydrogels. Soft Matter. **2013**, 9, 10287.
58. Ji D; Park J. M.; Oh M. S.; Nguyen T. L.; Shin H; Kim J. S.; Kim D; Park H. S.; Kim J. Superstrong, superstiff, and conductive alginate hydrogels. Nat. Commun. **2022**, 13, 3019.
59. Zhang L. L.; Zhao X. S. Carbon-based materials as supercapacitor electrodes. Chem. Soc. Rev. **2009**, 38, 2520-2531.
60. Meng X; Qiao Y; Do C; Bras W; He C; Ke Y; Russell T. P.; Qiu D. Hysteresis-Free Nanoparticle-Reinforced Hydrogels. Adv. Mater. **2022**, 34, 2108243.
61. Duan Z; Hou Y; Chang Y; Zhao Q; Guo M; Wu S; Zhou S; Ma Y. Low-temperature 3D-printing conductive hydrogel based sensing materials for highly sensitive soft strain sensors. Sensor. Actuat. A-Phys. **2025**, 389, 116571.
62. Abdurrahmanoglu S; Can V; Okay O. Design of high-toughness polyacrylamide hydrogels by hydrophobic modification. Polymer. **2009**, 50, 5449-5455.